Tectonophysics 582 (2013) 177–187

Contents lists available at SciVerse ScienceDirect

Tectonophysics

journal homepage: www.elsevier.com/locate/tecto

Crustal and uppermost mantle structure and seismotectonics of North China Craton

Jian Wang [a,*], Dapeng Zhao [b], Zhenxing Yao [a]

[a] Key Laboratory of the Earth's Deep Interiors, Institute of Geology and Geophysics, Chinese Academy of Sciences, Beijing, 100029, China
[b] Department of Geophysics, Tohoku University, Sendai, 980-8578, Japan

ARTICLE INFO

Article history:
Received 31 August 2011
Received in revised form 30 September 2012
Accepted 1 October 2012
Available online 12 October 2012

Keywords:
P-wave anisotropy
Seismic tomography
North China Craton
Crustal earthquakes
Fossil anisotropy
Seismotectonics

ABSTRACT

We determined a 3-D P-wave anisotropic tomography of the crust and uppermost mantle beneath North China Craton (NCC) using 107,976 P-wave arrival times from 16,073 local earthquakes recorded by 380 seismic stations. Our results show significant lateral heterogeneities beneath NCC. The lower crust and uppermost mantle beneath the North China Basin show widespread low-velocity anomalies which may reflect high-temperature materials caused by the late Mesozoic basaltic magmatism in the NCC. Low-velocity anomalies also exist beneath the Trans-North China Orogen, which may reflect asthenospheric upwelling since late Mesozoic. Large crustal earthquakes generally occurred in high-velocity zones in the upper to middle crust, while low-velocity and high-conductivity anomalies that may represent fluid-filled, fractured rock matrices exist in the lower crust to the uppermost mantle under the source zones of the large earthquakes. The crustal fluids may lead to the weakening of the seismogenic layer in the upper and middle crust and hence cause the large crustal earthquakes. The NW–SE P-wave fast velocity directions seem to be dominant in the uppermost mantle under the central parts of eastern NCC, suggesting that these mantle minerals were possibly regenerated but keep the original fossil anisotropy formed before the new lithospheric mantle was produced during the Mesozoic to Cenozoic.

1. Introduction

Cratons are the stable tectonic units characterized by a cold and thick lithosphere keel. Different from other cratons having thick lithosphere of ~200 km, such as the Kaapvaal craton (Chevrot and Zhao, 2007; Fishwick, 2010), the North American craton (Frederiksen et al., 2001), and the Australia craton (Fichtner et al., 2010; Fishwick and Reading, 2008), the eastern North China Craton (NCC) is suggested to have experienced significant lithospheric thinning and modification during the Mesozoic–Cenozoic by examining the physical and chemical properties of the sub-continental lithospheric mantle (e.g., Griffin et al., 1998; Menzies and Xu, 1998; Zheng et al., 1998). Accordingly, the NCC, the Chinese part of the Sino-Korean Craton, is extraordinary that consists of a relatively intact western part and a destroyed eastern part, which are separated by the Central Orogenic Belt also known as the Trans-North China Orogen (TNCO) (Fig. 1) (Zhao et al., 2001). Traditionally, the NCC is described as a collage of two blocks (the eastern and western blocks) dissected by the TNCO (G. Zhao et al., 2005, 2009). However, recent studies (Santosh, 2010; Tsunogae et al., 2011) revealed that the western NCC is composed of two distinct sub-blocks termed the Ordos and Yinshan welded along the Inner Mongolia Suture Zone, rather than a uniform block.

The NCC has recently been paid much attention as a typical region to study the continental seismotectonics and geodynamics (e.g., Chen et al., 2006; Fan et al., 2000; Gao et al., 2002; Wu et al., 2005; Xu et al., 2004; Zhai and Liu, 2003; Zhang et al., 2004; Zheng et al., 2009; Zhu and Zheng, 2009). Seismic tomography is one of the most powerful tools to study the three-dimensional (3-D) velocity structure beneath North China and its adjacent areas (e.g., Chang et al., 2007; Huang and Zhao, 2004, 2006, 2009; Priestley et al., 2006; Qi et al., 2006; Tian and Zhao, 2011; Tian et al., 2009; Xu and Zhao, 2009). Seismic tomography clearly imaged the high-velocity (high-V) subducted Pacific slab stagnating in the mantle transition zone beneath the eastern NCC (Huang and Zhao, 2006; Zhao, 2004). A high-V root extending down to about 200 km depth beneath the western NCC is revealed (Tian and Zhao, 2011; Tian et al., 2009; Xu and Zhao, 2009). In addition, a high-V anomaly is detected atop the 410 km discontinuity beneath the eastern NCC, which may reflect the delaminated lithosphere (Huang and Zhao, 2009; Xu and Zhao, 2009). Recently, Santosh et al. (2010) investigated the mantle dynamics of the Paleo-proterozoic NCC by synthesizing the recent tomographic images (Tian et al., 2009; Xu and Zhao, 2009) and their correlation with the surface geological features in NCC. However, the seismic velocity structure of the crust and upper mantle has been assumed to be isotropic in these previous tomographic studies.

Shear-wave splitting measurements reveal that seismically anisotropic materials are common in the Earth's interior (for reviews, see Helbig and Thomsen, 2005; Maupin and Park, 2007; Savage, 1999). Seismic anisotropy can record very important information for studying the present or past tectonic deformation in the Earth (Savage, 1999; Silver, 1996). Recently, Zhao and Xue (2010) studied

* Corresponding author. Tel.: +86 10 82998600; fax: +86 10 62010846.
E-mail address: jianwang@mail.iggcas.ac.cn (J. Wang).

0040-1951/$ – see front matter © 2012 Elsevier B.V. All rights reserved.
http://dx.doi.org/10.1016/j.tecto.2012.10.004

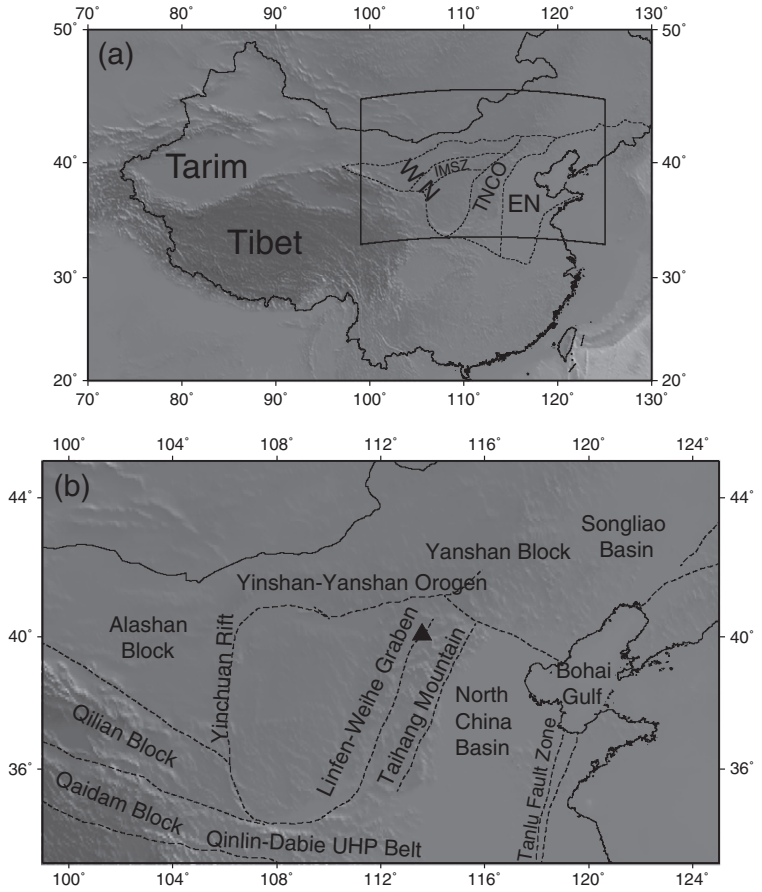

Fig. 1. (a) Map showing the major geological features of China and surrounding regions. The black box shows the location of the present study area. The dashed lines show the major tectonic units of the NCC (after Santosh, 2010; Zhao et al., 2001). EN, the Eastern NCC; WN, the Western NCC; TNCO, the Trans-North China Orogen; IMSZ, Inner Mongolia Suture Zone. (b) Tectonic background of the NCC. The dashed lines show the major faults or block boundaries (after Tian et al., 2009; Zhao et al., 2005). The black triangle denotes the Datong volcano group. The maps are plotted on a color background of the Asia topography (gtopo30).

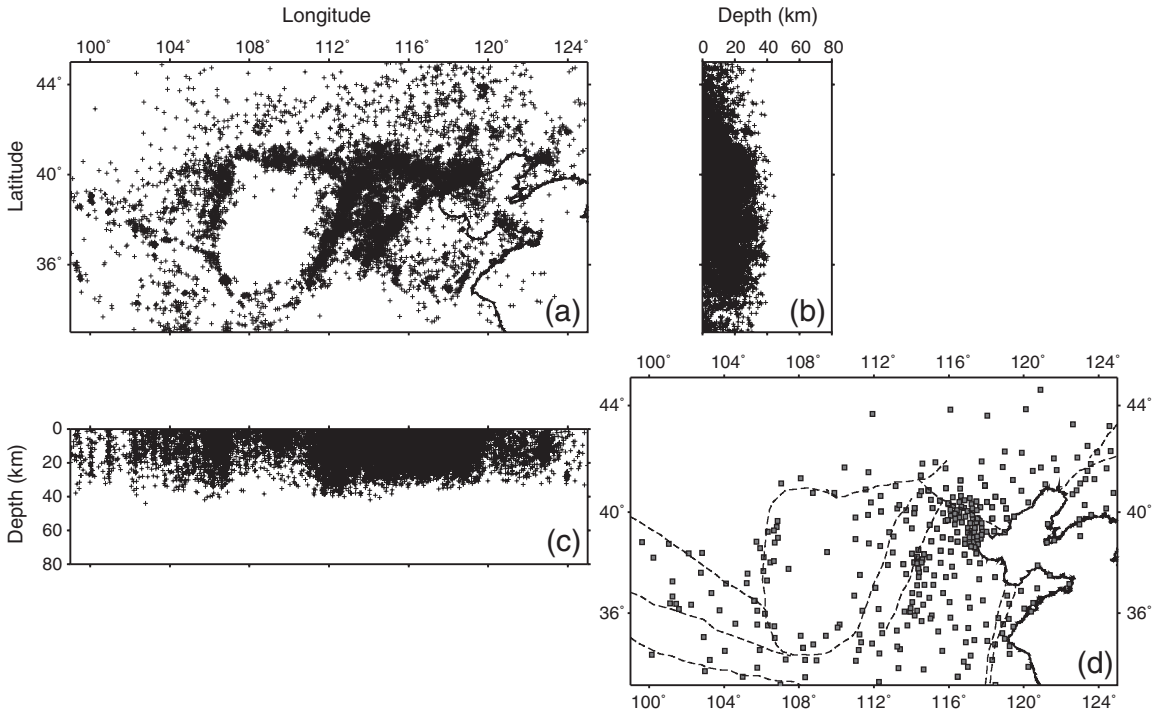

Fig. 2. (a-c) Hypocenter distribution of 16,073 local earthquakes (crosses) used in this study. (d) Distribution of 380 seismic stations (gray squares) used in this study. The dashed lines show the major faults or block boundaries as shown in Fig. 1b.

the mantle flow pattern of the NCC reactivation using the SKS splitting measurements and proposed a hybrid mantle flow model beneath NCC, and they suggested that a mantle-wedge flow exists beneath the eastern NCC and a regional upwelling exists beneath the TNCO. Although shear-wave splitting measurement is useful to estimate the seismic anisotropy on a nearly vertical path of S wave, its depth resolution is poor to distinguish the anisotropic bodies at depths. In addition, the incident angle of S wave at a seismic station should be considered. In contrast to the S-wave splitting observations, P-wave travel time data with various ray paths are capable of imaging both lateral velocity variation and anisotropy (e.g., Eberhart-Phillips and Henderson, 2004; Eberhart-Phillips and Reyners, 2009; Hearn, 1996; Hirahara and Ishikawa, 1984; Ishise and Oda, 2005, 2008; Smith and Ekstrom, 1999; Wang and Zhao, 2008, 2010, 2012). In this work, we have determined

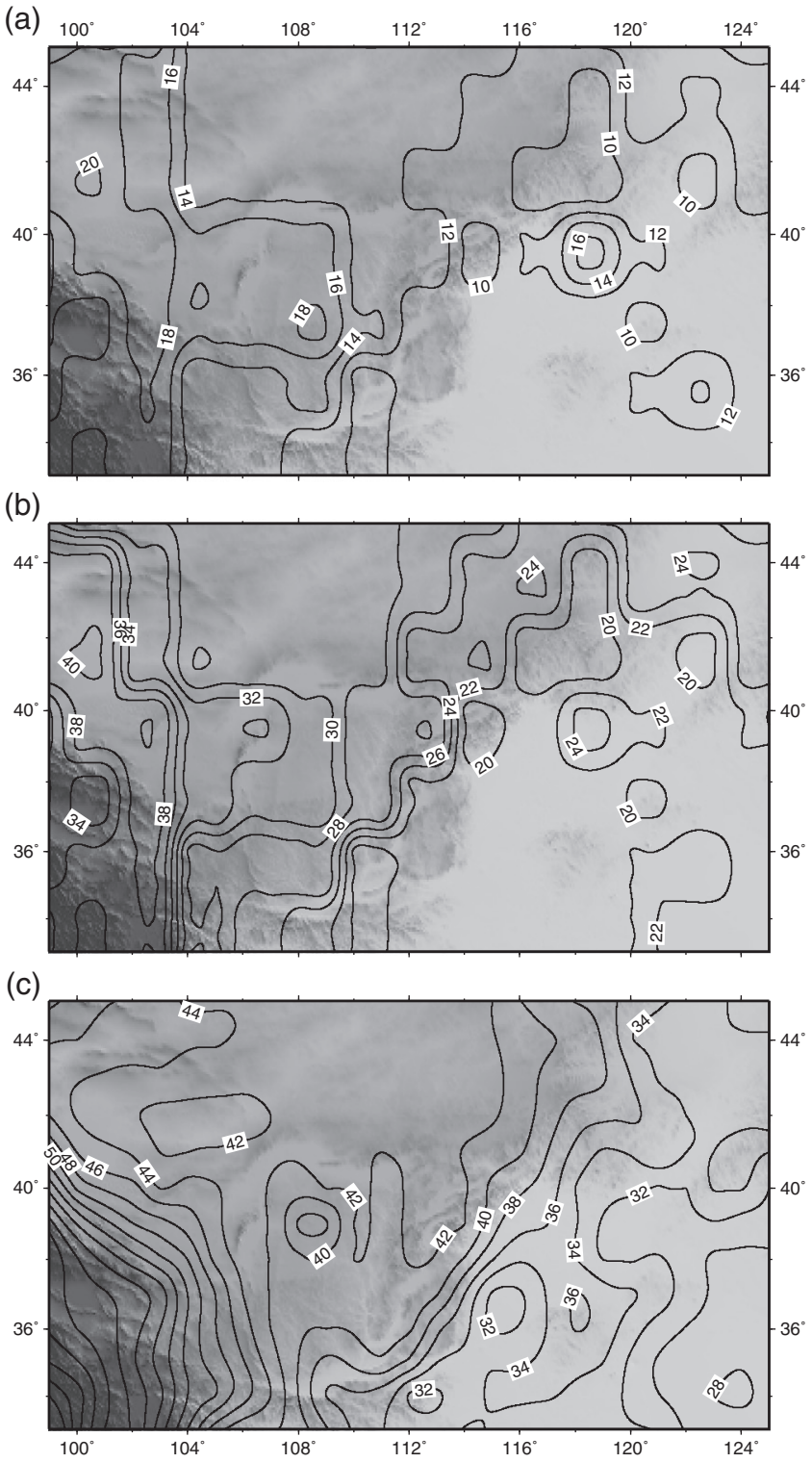

Fig. 3. The crustal model used in this study. (a–b) Depth variations of the upper and middle crust beneath the NCC from the CRUST2.0 model. (c) Moho depth variation beneath the NCC used in this study, which is digitized from Cai et al. (2007). The maps are plotted on a gray background of the Asia topography (gtopo30).

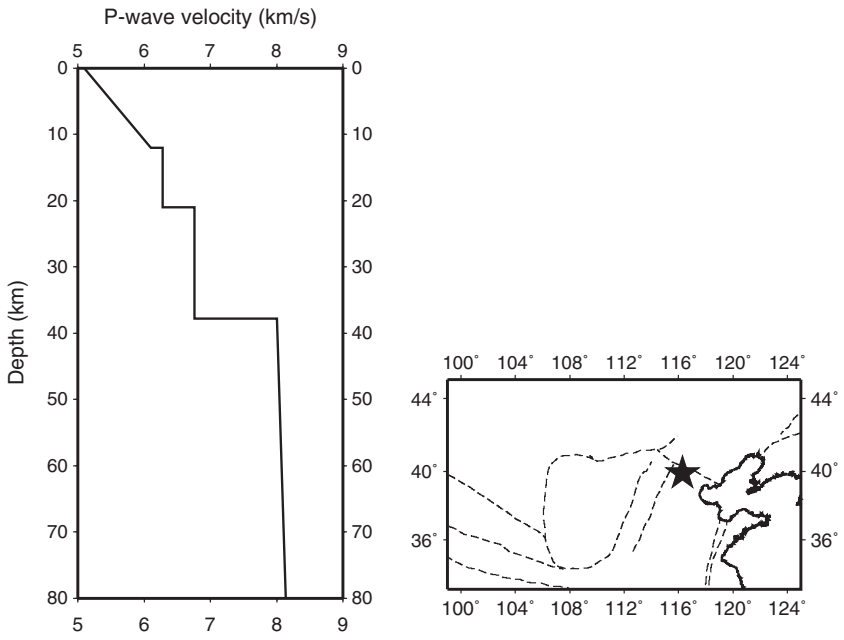

Fig. 4. The starting 1-D P-wave velocity model (solid line) under the area shown with a star symbol. It is modified from Huang and Zhao (2004) in accord with the crustal model used in this study.

3-D P-wave anisotropic tomography of the crust and uppermost mantle under NCC to study the seismotectonics and geodynamics of the region.

2. Method and data

Ishise and Oda (2005) improved the method of Hirahara and Ishikawa (1984) to perform a seismic tomography for both isotropic and anisotropic velocity structures beneath Northeast Japan. Eberhart-Phillips and Henderson (2004) modified the technique of Hearn (1996) to estimate the 3-D velocity structure including azimuthal anisotropy in New Zealand using P-wave travel time data. Similar to these studies, Wang and Zhao (2008) modified the isotropic tomographic program (TOMOG3D) of Zhao et al. (1992) to invert for both 3-D P-wave velocity variation and azimuthal anisotropy in

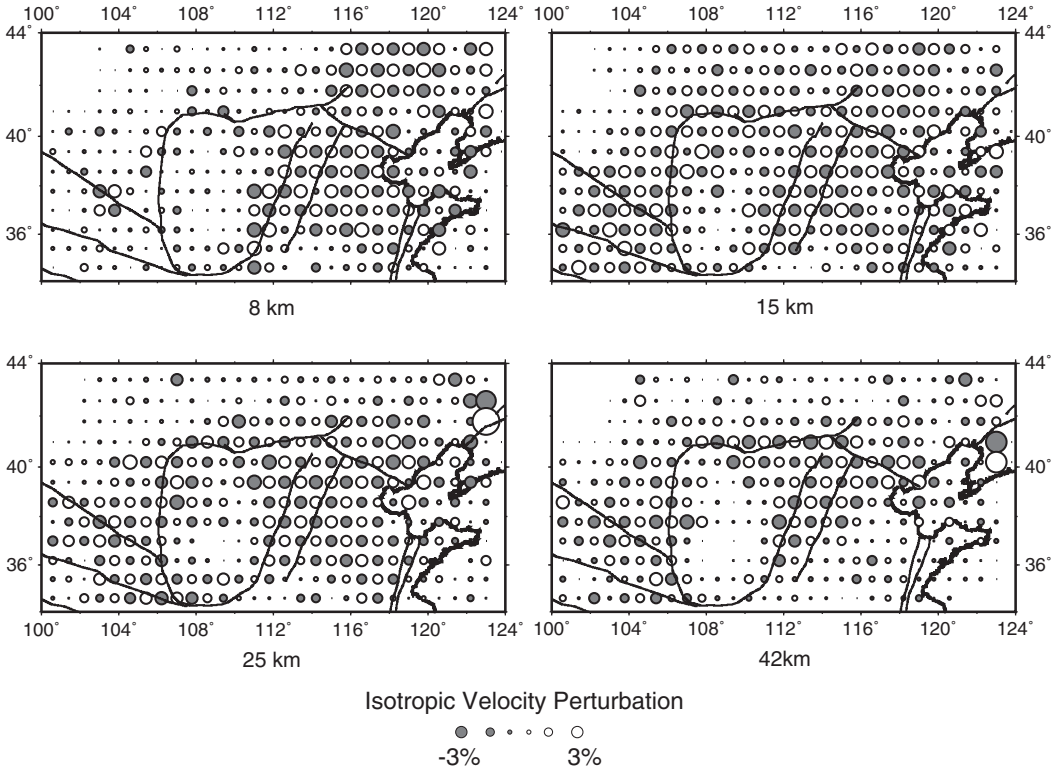

Fig. 5. Output results of isotropic velocity perturbations at four depths for the checkerboard resolution test. The input model is that the isotropic velocity anomalies of ±3% are assigned to the 3-D grid nodes. Black and white circles denote low and high velocity perturbations, respectively. The black lines show the major faults or block boundaries as shown in Fig. 1b.

Northeast Japan. Their method was further improved by considering the azimuthal coverage of rays for anisotropy (Wang and Zhao, 2010) and adopting two independent grids for isotropic and anisotropic velocity structures (Wang and Zhao, 2012). In this work we used the anisotropic tomography method of Wang and Zhao (2012) for studying the 3-D velocity variations and azimuthal anisotropy in the crust and uppermost mantle beneath NCC.

In the inversion, we used 107,976 P-wave arrival times with residual less than 1.0 s from 16,073 local earthquakes recorded by 380 seismic stations during January 1986 to December 2008 (see Fig. 2). These arrival-time data were collected from Reports of the Beijing Digital Telemetry Seismic Network during 2001 to 2007, and phase database of China Earthquake Data Center during 1986 to 2008. Among many thousands of earthquakes in the original data set, the events used in this study were selected carefully based on the following criteria: (1) all the selected events were recorded by more than 8 seismic stations; (2) they have reliable hypocentral locations with uncertainties <5 km; and (3) they are selected to keep a uniform distribution of hypocenters in the study area. Although an effort was made to keep a uniform distribution of hypocenters, the selected events are actually not distributed uniformly because seismicity is very low in some areas such as the Ordos plateau.

Following Wang and Zhao (2010), we used a parameter MRAGA (maximum ray-azimuth gap angle), which is deduced from the azimuths of the rays passing through each grid node, as a constraint to the anisotropic inversion. After many resolution tests we found that the optimal grid spacing was 0.8° in the horizontal direction for determining both isotropic velocity variation and anisotropy. In this study, the isotropic velocity perturbation was inverted only for the grid nodes with at least 8 passing rays, and anisotropy was inverted only for the grid nodes with at least 8 passing rays and with MRAGA<25°. Four grid meshes were set at depths of 8, 15, 25 and 42 km for the isotropic velocity inversion, while three grid meshes were set at depths of 5, 20 and 45 km for the anisotropic inversion.

Lateral variations in the thickness of the upper, middle and lower crust were taken into account in the model. Because there is no proper local crustal model in NCC, lateral depth variations of the upper and middle crust were taken from the global crustal model CRUST 2.0 (see Fig. 3a and b), which was specified on a 2°×2° cell (Bassin et al., 2000). We used the Moho depth variation determined by Cai et al. (2007) for China and its adjacent regions, which was digitized on a 1°×1° cell in this study (see Fig. 3c). The geometries of the three velocity discontinuities were fixed in the inversion process. Many previous studies have shown that ray paths and travel times can be computed more accurately when the discontinuity geometries are taken into account (e.g., Huang and Zhao, 2004; Qi et al., 2006; Wang and Zhao, 2008; Zhao et al., 1992). The LSQR algorithm (Paige and Saunders, 1982) was applied to solve the large but sparse system of observation equations. The nonlinear tomographic problem was solved by iteratively conducting linear inversions. The final results were obtained after four iterations. Considering the trade-off between the velocity model norms and the root mean square (RMS) of travel-time residuals, the damping parameters were 4, 25, 50, and 100 during the iterations, respectively. Smoothing regularization was applied in the inversion, and after many real inversions the smoothing parameters for the velocity perturbation and anisotropy were chosen to be 0.0025 and 0.01, respectively. The RMS of travel-time residuals, which was 0.50 s for the initial model, was reduced to 0.36 s for isotropic tomography and 0.35 s for anisotropic tomography, respectively, upon optimization. Recent studies (e.g., Fichtner et al., 2010; Nettles and Dziewonski, 2008) suggested that the anisotropy would change substantially when the non-linear effects are accounted for through the iterative improvement of the inversion in surface-wave and full-waveform tomography. In this work we ignored the non-linear effects in our P-wave travel-time anisotropic tomography.

3. Resolution

Similar to our previous studies of anisotropic tomography in Japan (e.g., Wang and Zhao, 2010, 2012), we adopted the checkerboard resolution test (CRT) to evaluate the resolution of the tomographic images. CRT is a convenient and well-used tool to make resolution analysis in tomographic inversions (e.g., Leveque et al., 1993; Thurber and Ritsema, 2007). The starting P-wave isotropic velocity model is shown in Fig. 4, which was modified from Huang and Zhao (2004) to be in accord with the crustal model of this study. Isotropic velocity anomalies of ±3% were alternatively assigned to the nodes of the grid net for isotropic velocity perturbation. The FVDs at two adjacent grid nodes were perpendicular to each other (22.5° and 112.5°), and the amplitude of anisotropy was 4.25%. Random errors in a normal distribution with a standard deviation of 0.15 s are added to the theoretical arrival times calculated for the synthetic model. Then we inverted the synthetic data with the same algorithm as for the real data by using the starting velocity model shown in Fig. 4. The resolution is considered to be good for areas where the checkerboard

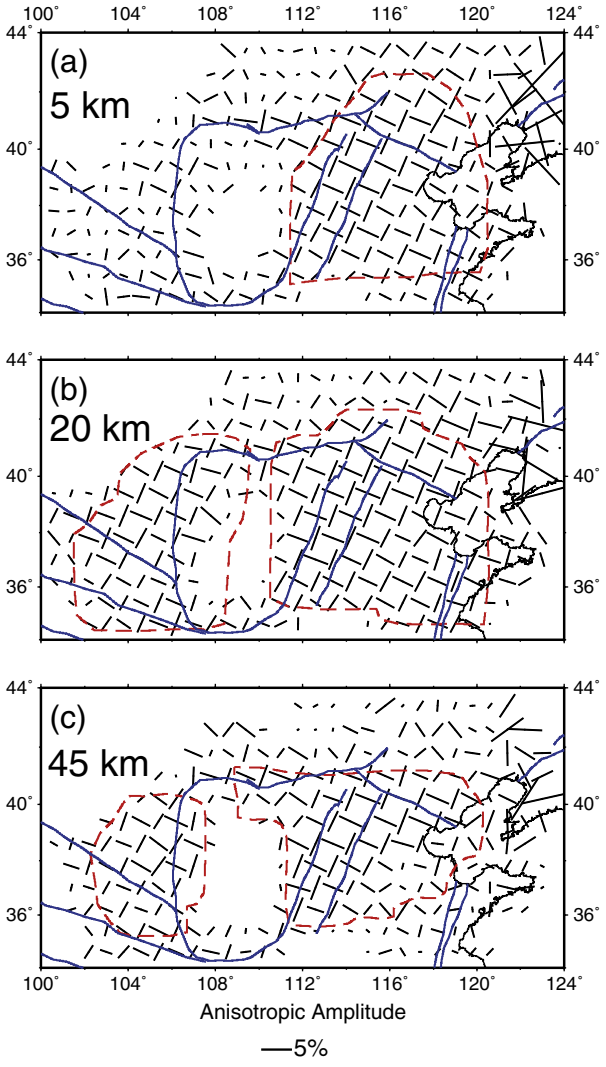

Fig. 6. Output results of P-wave anisotropy at three depths for the checkerboard resolution test. The input model is that the FVDs at two adjacent grid nodes are perpendicular to each other (22.5° and 112.5°), and the amplitude of anisotropy is 4.25%. Azimuth and length of bars represent the FVD and anisotropic amplitude, respectively. The enclosed red lines show the areas where the anisotropy is well recovered. The blue lines show the major faults or block boundaries as shown in Fig. 1b.

image is recovered. Figs. 5 and 6 show the CRT results for isotropic velocity perturbations and anisotropic structure, respectively. The resolution is generally good in most parts of the study area for isotropic velocity perturbations except for the Ordos plateau because of the lack of earthquakes and stations there. In the areas enclosed by the red lines shown in Fig. 6, the FVDs are well recovered with small errors in anisotropic amplitudes.

Many studies (e.g., Backus, 1962; Capdeville et al., 2010; Fichtner et al., 2010) suggested that there is a very strong trade-off between seismic heterogeneity and anisotropy. Hence we conducted four more tests to investigate the influence of the trade-off on our inversion results. The isotropic velocity anomalies were changed to ±6% and the anisotropic amplitude varied from 0 to 4.25% in the input model of these tests. Results of the four tests indicate that the anisotropic structure is well recovered in the areas enclosed by the red lines (Figs. S2, S4, S6, and S8), suggesting that the inverted anisotropy is less affected by the unrevealed heterogeneity and the resolution is mainly influenced by the ray coverage in our P-wave anisotropic tomography (for detail, please see the online Supporting material). Although these tests show good resolution of our tomographic model, the results should be interpreted with caution by taking into account information from other studies with different approaches.

4. Results and discussion

The isotropic velocity images show significant lateral heterogeneities in the crust and uppermost mantle beneath NCC (Figs. 7 and 8). The pattern of the anisotropic structure is complex and varies at different depths (Fig. 9). Fig. 10 show the tomographic images determined by inverting the same data set (Fig. 2) and crustal model (Fig. 3) for only the isotropic velocity tomography. Comparing the images with those shown in Fig. 8, we can see that the velocity images in the two results are generally similar, while some changes appear, in particular, at latitudes 41.0° and 40.2°. At latitude 41.0°, the eastern high-V anomaly in the lower crust and uppermost mantle in Fig. 10a is obviously stronger than that shown in Fig. 8a, and at latitude 40.2° the image of the high-V anomaly in the lower crust and uppermost mantle varies around longitude 110°. The results suggest that the isotropic P-wave velocity images have slight changes when the azimuthal anisotropy is taken into account in the inversion, which is expected.

4.1. Velocity heterogeneities

Fig. 7 shows the obtained isotropic velocity tomography at four depths beneath NCC. High-V anomalies (H0) are visible beneath the northern part of the North China Basin (NCB) at 8 km depth, which is consistent with the result of Tian et al. (2009). In the lower crust and uppermost mantle beneath the NCB (25 and 42 km depths) widespread low-V anomalies are visible, being generally consistent with the result of Chang et al. (2007) and the Pn velocity image by Liang et al. (2004). The widespread distribution of low-V zones suggests that the lower crust contains high-temperature materials caused by the late Mesozoic basaltic magmatism in the NCC (Fan et al., 2000; Menzies and Xu, 1998). Thus, the high-temperature in the lower crust provides an appropriate condition for large-scale ore-forming processes in the NCC (Chang et al., 2007). The Tan-Lu fault is characterized by a low-V zone (L1 in Fig. 7), which possibly reflects asthenospheric upwelling in this region. A high-V anomaly (H2 in Fig. 7) is clearly imaged beneath the area between the Yanshan block and Songliao basin. A high-V anomaly was imaged by Tian et al. (2009), and a high-Vs zone was imaged by Lebedev and Nolet (2003) in the same region. As suggested by Tian et al. (2009), the high-V anomaly may be related to an Archean-Early Proterozoic mantle terrane beneath the Songliao basin extending to the west (Zhang et al., 1998). A prominent low-V anomaly (L2 in Fig. 7) with NE-SW trend is visible in the crust and uppermost mantle beneath the TNCO. The previous studies revealed a low-V anomaly beneath the TNCO down to ~300 km depth (Tian et al., 2009) and even to ~500 km depth (L. Zhao et al., 2009). Magmatic events have occurred frequently in the TNCO since late Mesozoic, and most of the known Cenozoic basalts are located in the region (Wu et al., 2008). Thus,

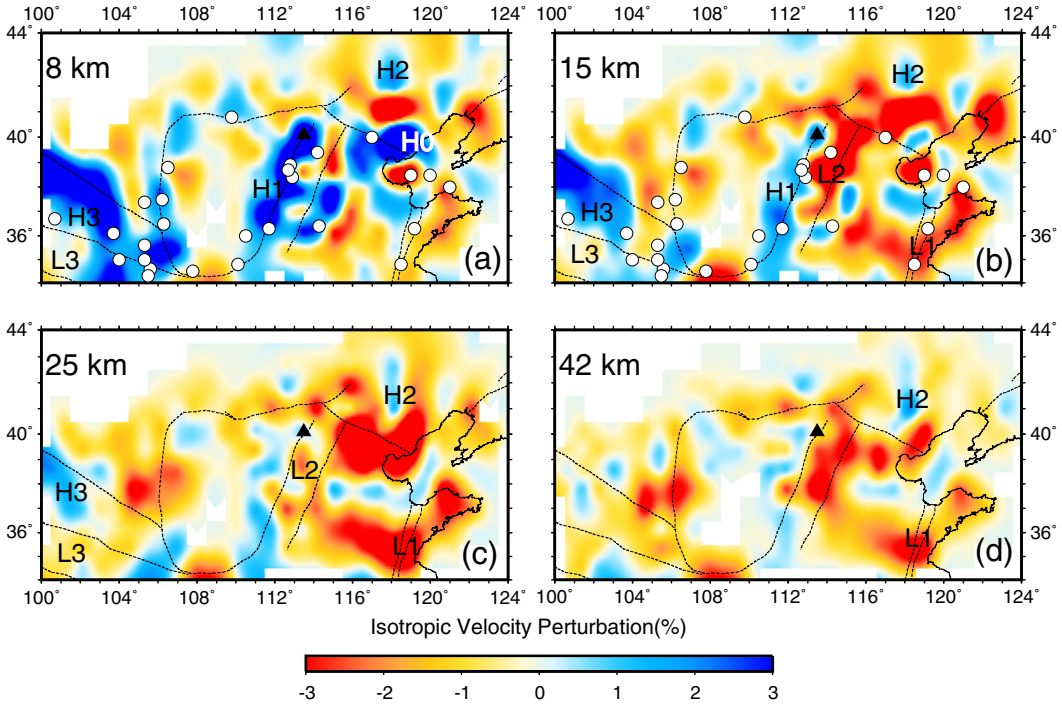

Fig. 7. The obtained isotropic velocity images at four depth layers. The dashed lines denote the major faults or block boundaries as shown in Fig. 1b. The black triangle denotes the Datong volcano group. White circles denote the large historic earthquakes ($Ms \geq 7.0$) occurred in this region during BC 780 to AD 1900. Red and blue colors denote low and high velocities, respectively.

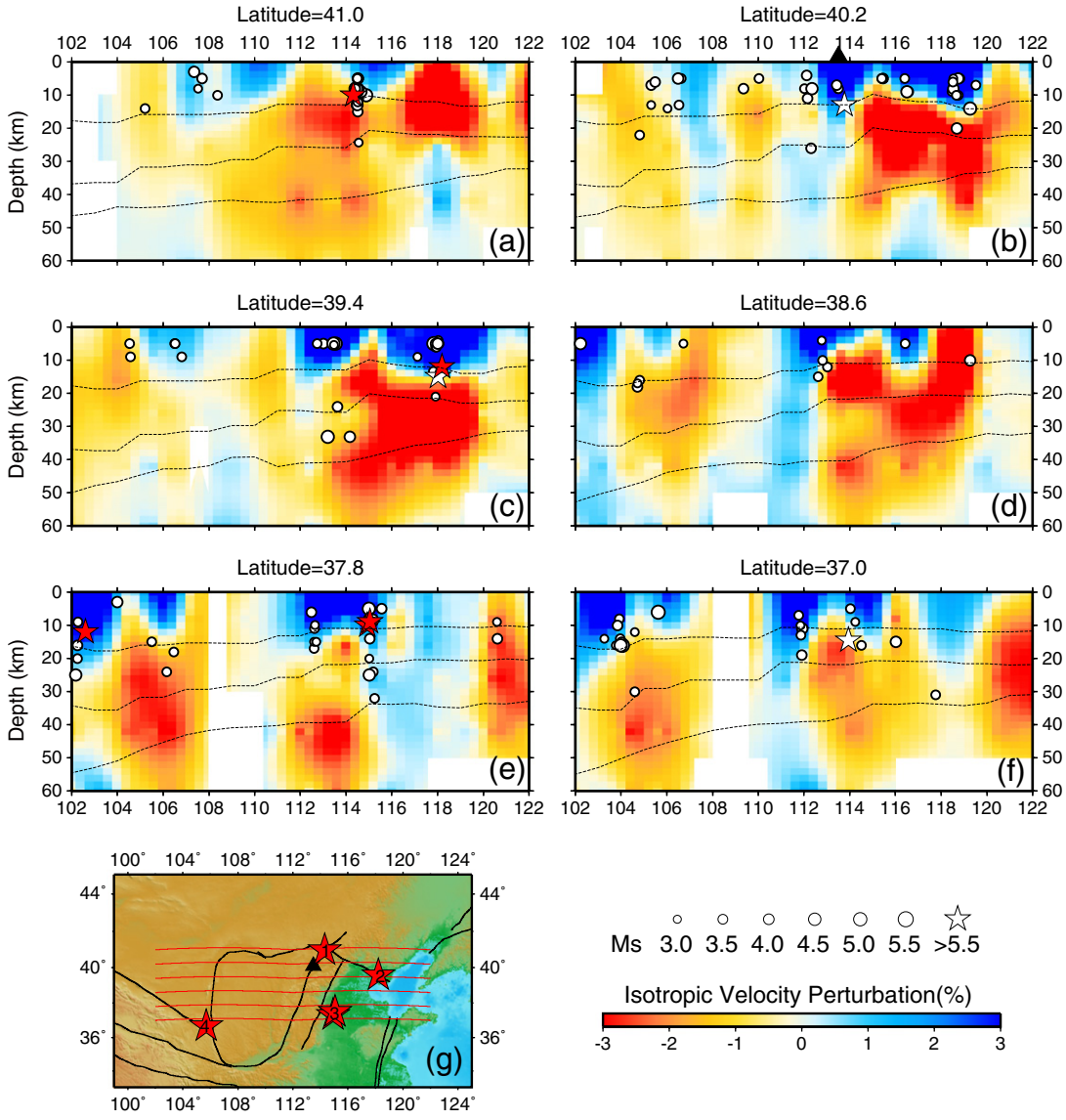

Fig. 8. Vertical cross sections of isotropic velocity images along six profiles shown in (g). The dashed lines show depths of the upper, middle and lower crust, respectively. White circles and stars denote the earthquakes of $3.0<Ms\leq5.5$ and $M>5.5$, respectively, which occurred within a 20 km width along each profile. The black triangle denotes the Datong volcano group. The red star in panel a (red star 1 in panel g) denotes the 1998 Zhangbei-Shangyi earthquake (Ms 6.2). The red star in panel c (red star 2 in panel g) denotes the 1976 Tangshan earthquake (Ms 7.8). As shown in panel e, two adjacent red stars (red stars 3 in panel g) denote the 1966 Xingtai earthquakes (*Ms* 6.8 and *Ms* 7.2), and the individual red star (red star 4 in panel g) denotes the 1927 Gulang earthquake (Ms 8.0). Red and blue colors denote low and high velocities, respectively.

the low-V anomaly may reflect the magmatic activity and asthenospheric upwelling beneath the TNCO since late Mesozoic. A prominent high-V anomaly (H1 in Fig. 7) is visible beneath the Datong volcanic area, which is consistent with the high Rayleigh-wave group velocity from ambient-noise tomography (Fang et al., 2010). Our results suggest that the Datong volcano group may be inactive now, and so it is different from the active Wudalianchi and Changbai volcanoes in Northeast China (D. Zhao et al., 2004, 2009). The resolution of the tomographic image is lower within the Ordos plateau due to the lack of earthquakes and seismic stations there. A prominent high-V anomaly (H3 in Fig. 7) exists beneath the Qilian block in the upper and middle crust, while a low-V anomaly (L3 in Fig. 7) is visible beneath the Qaidam basin, which is consistent with the previous results (Guo et al., 2004; Xu et al., 2001). The Qilian block is a tectonically active region with a high level of seismicity, and it is composed of the Paleozoic and even Archean strata with high velocities. But the Qaidam basin is composed of the Mesozoic and Cenozoic sedimentary deposits, where the seismic velocities are low.

The white circles in Fig. 7a and b denote the hypocenter locations of the large historic earthquakes ($Ms\geq7.0$) that occurred in this region during BC 780 to AD 1900. This region has a long history of civilization and hence has detailed earthquake records in China. Although the accurate focal depths of these large historic earthquakes are unknown, a statistic analysis of the modern seismicity suggested that most of the large earthquakes occur mainly at 10–15 km depths in this region (Zang and Yang, 1984). As shown in Fig. 7a and b, most of the large earthquakes occurred in the major fault zones or the block boundaries. In the tomographic images at 8 and 15 km depths, we can see that most of the large earthquakes are located in high-V zones and close to the boundary between the low-V and high-V anomalies, which is consistent with many previous tomographic results in different regions and tectonic settings (e.g., Hauksson and Haase, 1997; Huang and Zhao, 2004; Qi et al., 2006; Zhao et al., 2010).

Fig. 8 shows six vertical cross sections of isotropic velocity images. The white circles and stars denote the earthquakes of $3.0<Ms\leq5.5$ and $Ms>5.5$, respectively, that occurred within a 20 km width

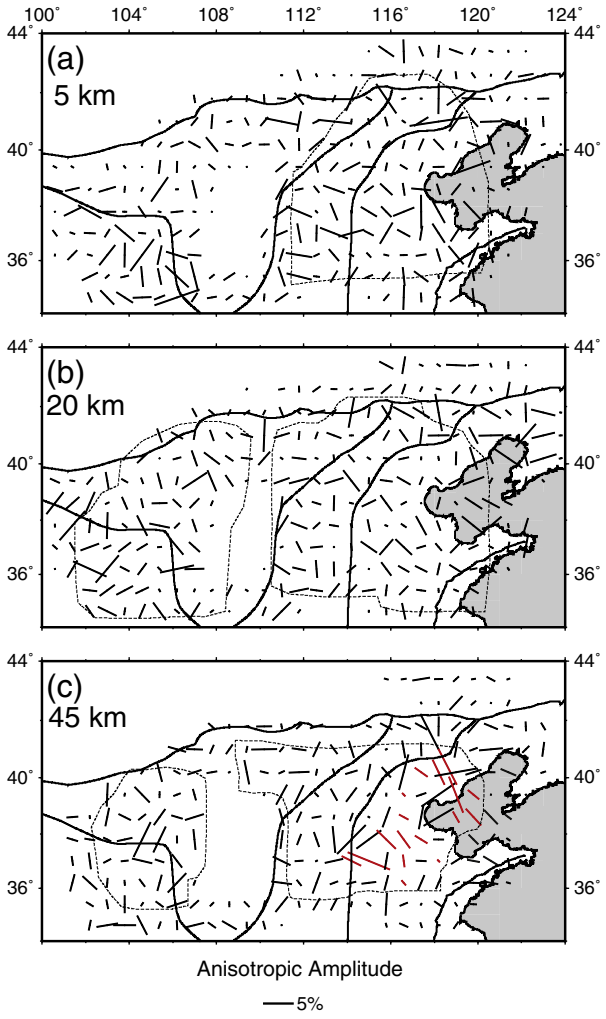

Fig. 9. The obtained P-wave anisotropic images at three depth layers. The dashed lines show the well-recovered areas as revealed by the CRTs. The azimuth and length of bars represent the FVD and anisotropic amplitude, respectively. Red bars denote the NW–SE FVDs beneath the eastern NCC (see text for details).

along each profile. Most of the events occurred in the upper and middle crust with focal depths shallower than about 20 km, and most of the events are located in high-V areas, although some are in low-V areas or at the boundary between the high-V and low-V areas. The larger earthquakes (white stars, $Ms > 5.5$) are generally located in high-V zones and close to the boundary between the high-V and low-V anomalies.

The 1998 *Ms* 6.2 Zhangbei-Shangyi earthquake (red star in Fig. 8a) is located above a low-V zone, which is consistent with the result by Chang et al. (2007). As shown in Fig. 8b, a prominent high-V anomaly with seismic events is visible in the crust beneath the Datong volcanic area. The 1976 *Ms* 7.8 Tangshan earthquake (red star in Fig. 8c) is located in a high-V zone in the upper to middle crust. Right beneath the high-V anomaly there is a prominent low-V zone in the lower crust and uppermost mantle. Liu et al. (1989) revealed a high-conductivity anomaly in the lower crust beneath the Tangshan area using magnetotelluric soundings. The high-conductivity and low-velocity anomaly in the lower crust beneath the Tangshan area may indicate the existence of fluids in the earthquake source area (e.g., Huang and Zhao, 2004, 2009; Qi et al., 2006). Similar high-conductivity and low-V anomalies have been found in the source areas of the 1995 Kobe earthquake in Japan (Zhao et al., 1996), and the 2001 Bhuj earthquake in India (Mishra and Zhao, 2003). The Xingtai earthquake sequence (two adjacent red stars in Fig. 8e) consisted of two large earthquakes: one (*Ms* 6.8) occurred on March 8, 1966, and the other (*Ms* 7.2) occurred on March 22, 1966. The two large earthquakes occurred in a high-V zone in the upper crust, while a prominent low-V anomaly exists in the lower crust and uppermost mantle. The 1927 *Ms* 8.0 Gulang earthquake (a red star in Fig. 8e) is located in a high-V zone, with a prominent low-V anomaly existing in the crust and uppermost mantle. The low-V anomalies under these large earthquakes may represent high-temperature anomaly or fluid reservoirs, which may lead to the weakening of the seismogenic layer in the upper and middle crust and hence caused the large crustal earthquakes (Zhao et al., 1996, 2010).

4.2. Anisotropy in the crust and uppermost mantle

Fig. 9 shows the obtained P-wave anisotropic structure at three depths beneath NCC. The dashed lines denote the areas where the obtained anisotropic images are well recovered by the synthetic tests as mentioned above. The results at 5 km and 20 km depths (Fig. 9a and b) display very complex patterns of anisotropy in the crust. We think that the grid interval of 0.8° in the horizontal direction in the tomography is too large to distinguish the small-scale anisotropy, which is induced by microcracks, cracks and lattice preferred orientation (LPO) of mineral crystals in crust (Godfrey et al., 2000; Kaneshima, 1990; Kern, 1993).

Mineral physics studies showed that olivine in the mantle peridotite xenoliths in the eastern NCC and the TNCO contains little water (Yang et al., 2008). Thus, the P-wave and S-wave FVDs in the mantle, which are mainly caused by the strain-induced LPO of olivine, are sub-parallel to the flow direction in the dry conditions (Karato et al., 2008; Katayama et al., 2004). In the uppermost mantle, the NW–SE P-wave FVDs seem to be dominant in central parts of the eastern NCC (denoted by red bars in Fig. 9c), while they become complex beneath the central and western NCC.

There are three possible ways to explain these dominant NW–SE P-wave FVDs. First, the anisotropy can be interpreted as a record for the deformation of the Paleozoic lithospheric mantle at the time of the formation and stabilization of the NCC. That is, these mantle materials are the Paleozoic lithospheric mantle and their anisotropy remain unchanged up to the present. However, the anisotropic feature of the Paleozoic lithospheric mantle under the eastern NCC is unknown. Second, these mantle materials are the Paleozoic lithospheric mantle but their anisotropy has been changed. However, The NW–SE FVDs are inconsistent with the seismic anisotropy resulted from the matching of North China and Yangtze cratons during Triassic, and from the collision of the Siberian and North China blocks during Permian–Triassic (Zhao and Xue, 2010). The Paleozoic lithospheric mantle is refractory and its anisotropy can hardly be changed. Even if the anisotropy of Paleozoic lithospheric mantle is changed, it may just occur at the collision zones but not under the central parts of the eastern NCC. Third, the NW–SE P-wave FVDs may record the deformation structure during the late Mesozoic to Cenozoic. The eastern NCC has experienced significant lithospheric thinning from a thick (~200 km) Archean or Proterozoic lithosphere (Griffin et al., 1998; Xu et al., 2004) to the present thin lithosphere (60–80 km) (Chen et al., 2006; Gao et al., 2002; Hu et al., 2000; Huang and Zhao, 2006). The refractory and enriched Paleozoic lithospheric mantle possibly had broadly been replaced by the fertile and depleted lithospheric mantle during the Mesozoic–Cenozoic in the eastern NCC, which is deduced from Re-Os isotopes and highly siderophile elements peridotite xenoliths of the NCC (e.g., Gao et al., 2002; Rudnick et al., 2011; Wu et al., 2006; Yang et al., 2010; Zheng et al., 2007). These NW–SE P-wave FVDs agree with the asthenosphere flow direction deduced from the SKS splitting observations in the eastern NCC (Huang et al., 2011; Zhao and Xue, 2010). Thus, the uppermost lithospheric mantle in the central parts of the eastern

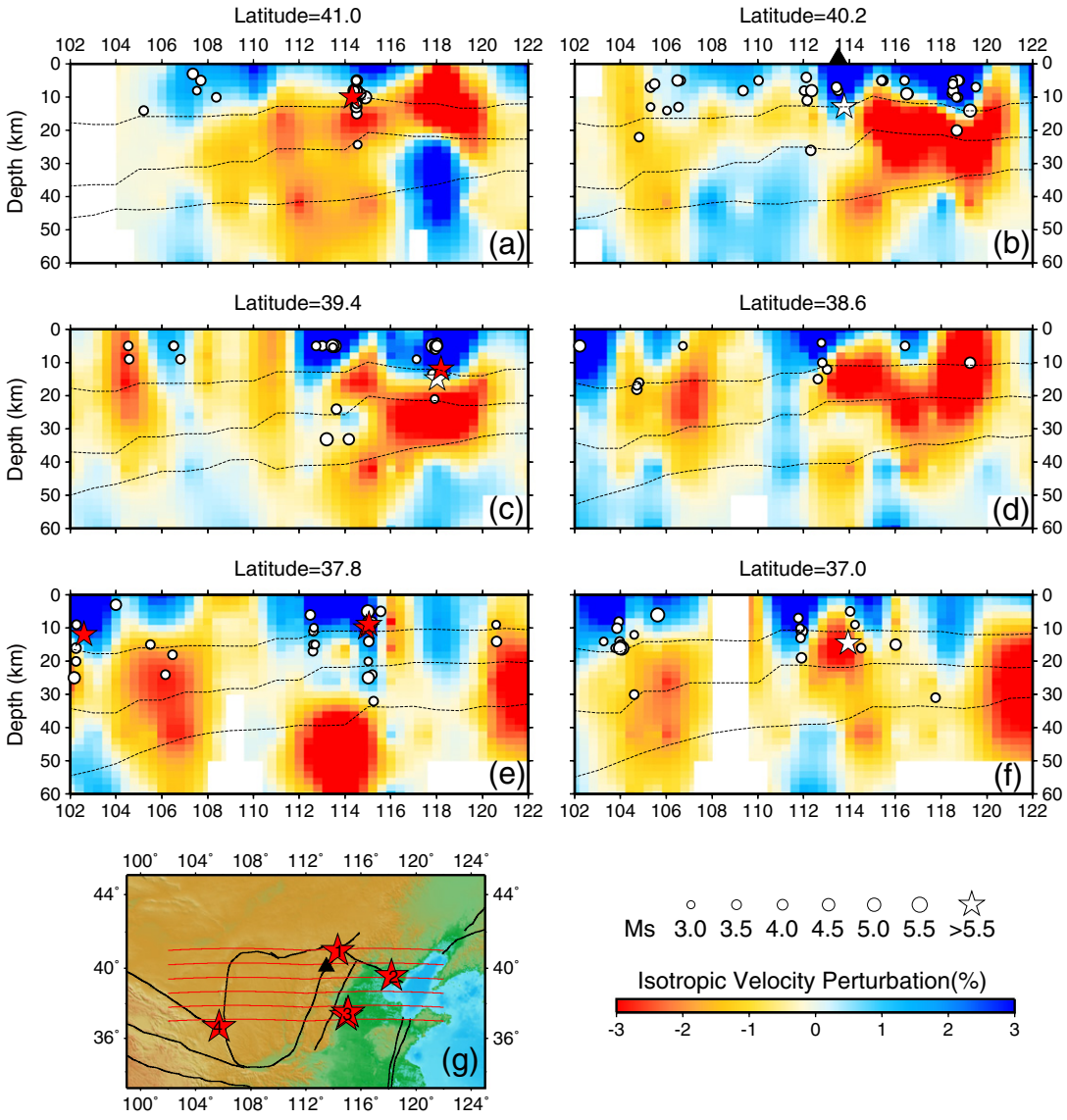

Fig. 10. The same as Fig. 8 but the images are obtained by inverting for the isotropic tomography alone.

NCC is characterized by the seismic anisotropy with the FVDs subparallel to the mantle flow direction in the big mantle wedge induced by the northwestward subduction of the Pacific plate under East Asia (Zhao et al., 2004, 2007). The result suggests that the uppermost lithospheric mantle possibly keeps the record of the deformation structure during the late Mesozoic to Cenozoic.

Therefore, we suggest that the uppermost lithospheric mantle under the central parts of the eastern NCC may keep the frozen-in anisotropy generated by the sub-lithospheric mantle flow associated with the lithospheric rejuvenation during the Mesozoic to Cenozoic. The Paleozoic lithosphere was destroyed and the upwelling asthenosphere formed the new lithosphere, then the new lithospheric mantle minerals keep the original fossil anisotropy aligned with the mantle flow during the Mesozoic to Cenozoic.

5. Conclusions

We determined P-wave anisotropic tomography of the crust and uppermost mantle beneath NCC. Widespread low-V anomalies are visible in the lower crust and uppermost mantle beneath the eastern NCC. Large crustal earthquakes generally occurred in high-V zones in the upper to middle crust, situated above the low-V anomalies in the lower crust to the uppermost mantle. The anisotropy is very complex in the crust beneath NCC probably because the tomography resolution is not high enough to distinguish the small-scale anisotropic structure induced by microcracks and cracks. Our results suggest that the uppermost lithospheric mantle under the central parts of the eastern NCC may keep the NW–SE frozen-in FVD generated by sub-lithospheric mantle flow associated with the lithospheric rejuvenation during the Mesozoic to Cenozoic.

Supplementary data to this article can be found online at http://dx.doi.org/10.1016/j.tecto.2012.10.004.

Acknowledgments

We thank the staff members of Beijing Digital Telemetry Seismic Network and China Earthquake Data Center for providing the P-wave arrival time data used in this study. We thank Prof. Jieshou Zhu for providing the map of crustal thickness distribution in China and its adjacent regions. The discussions with Prof. Liang Zhao were very helpful. We thank Prof. Hans Thybo (Editor in Chief), Dr. Andreas Fichtner and an anonymous reviewer for their very helpful review comments.

This research was financially supported by the National Science Foundation of China to J. Wang (Grants 40974026, 90714012 and 41074060). J. Wang and D. Zhao were partially supported by the Global-COE Program of Earth and Planetary Science of Tohoku University. Figures were made using the GMT software (Wessel and Smith, 1998).

References

Backus, G.E., 1962. Long-wave elastic anisotropy produced by horizontal layering. Journal of Geophysical Research 67 (11), 4427–4440.
Bassin, C., Laske, G., Masters, G., 2000. The current limits of resolution for surface wave tomography in North America. EOS, Transactions of the American Geophysical Union 81, F897.
Cai, X., Zhu, J., Cao, J., Cheng, X., 2007. 3D structure and dynamic types of the lithospheric crust in continental China and its adjacent regions. Geology in China-Chinese Edition 34 (4), 543–557.
Capdeville, Y., Guillot, L., Marigo, J.J., 2010. 2-D non-periodic homogenization to upscale elastic media for P-SV waves. Geophysical Journal International 182 (2), 903–922.
Chang, X., Liu, Y., Zhai, M., Wang, Y., 2007. Crustal P-wave velocity distributions and metallotectonics around the North China Craton. In: Zhai, M., Windley, B., Kusky, T., Meng, Q. (Eds.), Mesozoic sub-continental lithospheric thinning under eastern Asia: Geological Society, London, Special Publications, pp. 293–302.
Chen, L., Zheng, T.Y., Xu, W.W., 2006. A thinned lithospheric image of the Tanlu Fault Zone, eastern China: constructed from wave equation based receiver function migration. Journal of Geophysical Research 111, B09312 http://dx.doi.org/10.1029/2005 JB003974.
Chevrot, S., Zhao, L., 2007. Multiscale finite-frequency Rayleigh wave tomography of the Kaapvaal craton. Geophysical Journal International 169 (1), 201–215.
Eberhart-Phillips, D., Henderson, C.M., 2004. Including anisotropy in 3-D velocity inversion and application to Marlborough, New Zealand. Geophysical Journal International 156 (2), 237–254.
Eberhart-Phillips, D., Reyners, M., 2009. Three-dimensional distribution of seismic anisotropy in the Hikurangi subduction zone beneath the central North Island, New Zealand. Journal of Geophysical Research 114, B06301 http://dx.doi.org/10.1029/2008 JB005947.
Fan, W.M., Zhang, H.F., Baker, J., Jarvis, K.E., Mason, P.R.D., Menzies, M.A., 2000. On and off the North China Craton: where is the Archaean keel? Journal of Petrology 41 (7), 933–950.
Fang, L.H., Wu, J.P., Ding, Z.F., Panza, G.F., 2010. High resolution Rayleigh wave group velocity tomography in North China from ambient seismic noise. Geophysical Journal International 181 (2), 1171–1182.
Fichtner, A., Kennett, B.L.N., Igel, H., Bunge, H.P., 2010. Full waveform tomography for radially anisotropic structure: new insights into present and past states of the Australasian upper mantle. Earth and Planetary Science Letters 290 (3–4), 270–280.
Fishwick, S., 2010. Surface wave tomography Imaging of the lithosphere-asthenosphere boundary beneath central and southern Africa? Lithos 120 (1–2), 63–73.
Fishwick, S., Reading, A.M., 2008. Anomalous lithosphere beneath the Proterozoic of western and central Australia: a record of continental collision and intraplate deformation? Precambrian Research 166 (1–4), 111–121.
Frederiksen, A.W., Bostock, M.G., Cassidy, J.F., 2001. S-wave velocity structure of the Canadian upper mantle. Physics of the Earth and Planetary Interiors 124 (3–4), 175–191.
Gao, S., Rudnick, R.L., Carlson, R.W., McDonough, W.F., Liu, Y.S., 2002. Re–Os evidence for replacement of ancient mantle lithosphere beneath the North China craton. Earth and Planetary Science Letters 198 (3–4), 307–322.
Godfrey, N.J., Christensen, N.I., Okaya, D.A., 2000. Anisotropy of schists: contribution of crustal anisotropy to active source seismic experiments and shear wave splitting observations. Journal of Geophysical Research 105 (B12), 27991–28007.
Griffin, W., Zhang, A., O'Reilly, S., Ryan, C., 1998. Phanerozoic evolution of the lithosphere beneath the Sino–Korean craton. In: Flower, M., Chung, S., Lo, C., Lee, T. (Eds.), Mantle dynamics and plate interactions in East Asia. Geodynamics Series. American Geophysical Union, pp. 107–126.
Guo, B., Liu, Q.Y., Chen, J.H., Zhao, D.P., Li, S.C., Lai, Y.G., 2004. Seismic tomographic imaging of the crust and upper mantle beneath the northeastern edge of the Qinghai-Xizang plateau and the Ordos area. Chinese Journal of Geophysics-Chinese Edition 47 (5), 790–797.
Hauksson, E., Haase, J.S., 1997. Three-dimensional V-P and V-P/V-S velocity models of the Los Angeles basin and central Transverse Ranges, California. Journal of Geophysical Research 102 (B3), 5423–5453.
Hearn, T.M., 1996. Anisotropic Pn tomography in the western United States. Journal of Geophysical Research 101 (B4), 8403–8414.
Helbig, K., Thomsen, L., 2005. 75th anniversary paper — 75-plus years of anisotropy in exploration and reservoir seismics: a historical review of concepts and methods. Geophysics 70 (6), 9nd–23nd.
Hirahara, K., Ishikawa, Y., 1984. Travel time inversion for 3-dimensional P-wave velocity anisotropy. Journal of Physics of the Earth 32 (3), 197–218.
Hu, S.B., He, L.J., Wang, J.Y., 2000. Heat flow in the continental area of China: a new data set. Earth and Planetary Science Letters 179 (2), 407–419.
Huang, J.L., Zhao, D.P., 2004. Crustal heterogeneity and seismotectonics of the region around Beijing, China. Tectonophysics 385 (1–4), 159–180.
Huang, J.L., Zhao, D.P., 2006. High-resolution mantle tomography of China and surrounding regions. Journal of Geophysical Research 111, B09305 http://dx.doi.org/10.1029/2005JB004066.
Huang, J.L., Zhao, D.P., 2009. Seismic imaging of the crust and upper mantle under Beijing and surrounding regions. Physics of the Earth and Planetary Interiors 173 (3–4), 330–348.
Huang, Z.C., Wang, L.S., Zhao, D.P., Mi, N., Xu, M.J., 2011. Seismic anisotropy and mantle dynamics beneath China. Earth and Planetary Science Letters 306 (1–2), 105–117.
Ishise, M., Oda, H., 2005. Three-dimensional structure of P-wave anisotropy beneath the Tohoku district, northeast Japan. Journal of Geophysical Research 110, B07304 http://dx.doi.org/10.1029/2004JB003599.
Ishise, M., Oda, H., 2008. Subduction of the Philippine Sea slab in view of P-wave anisotropy. Physics of the Earth and Planetary Interiors 166 (1–2), 83–96.
Kaneshima, S., 1990. Origin of crustal anisotropy — shear-wave splitting studies in Japan. Journal of Geophysical Research 95 (B7), 11121–11133.
Karato, S., Jung, H., Katayama, I., Skemer, P., 2008. Geodynamic significance of seismic anisotropy of the upper mantle: new insights from laboratory studies. Annual Review of Earth and Planetary Sciences 36, 59–95.
Katayama, I., Jung, H., Karato, S.I., 2004. New type of olivine fabric from deformation experiments at modest water content and low stress. Geology 32 (12), 1045–1048.
Kern, H.M., 1993. Physical-properties of crustal and upper-mantle rocks with regards to lithosphere dynamics and high-pressure mineralogy. Physics of the Earth and Planetary Interiors 79 (1–2), 113–136.
Lebedev, S., Nolet, G., 2003. Upper mantle beneath southeast Asia from S velocity tomography. Journal of Geophysical Research 108, B12048 http://dx.doi.org/10.1029/2000 JB000073.
Leveque, J.J., Rivera, L., Wittlinger, G., 1993. On the use of the checkerboard test to assess the resolution of tomographic inversions. Geophysical Journal International 115 (1), 313–318.
Liang, C.T., Song, X.D., Huang, J.L., 2004. Tomographic inversion of Pn travel times in China. Journal of Geophysical Research 109, B11304 http://dx.doi.org/10.1029/2003JB002789.
Liu, G., Sun, J., Liu, J., 1989. The electrical structure of the crust and upper mantle in North China. In: Ma, X. (Ed.), Lithospheric Dynamics ATLAS of China. China Cartographic Press, Beijing, pp. 59–62 (in Chinese).
Maupin, V., Park, J., 2007. 1.09 — Theory and Observations — Wave Propagation in Anisotropic Media. In: Gerald, S. (Ed.), Treatise on Geophysics. Elsevier, Amsterdam, pp. 289–321.
Menzies, M., Xu, Y., 1998. Geodynamics of the North China Craton. In: Flower, M., Chung, S., Lo, C., Lee, T. (Eds.), Mantle Dynamics and Plate Interactions in East Asia. Geodynamics Series. American Geophysical Union, pp. 155–165.
Mishra, O.P., Zhao, D.P., 2003. Crack density, saturation rate and porosity at the 2001 Bhuj, India, earthquake hypocenter: a fluid-driven earthquake? Earth and Planetary Science Letters 212 (3–4), 393–405.
Nettles, M., Dziewonski, A.M., 2008. Radially anisotropic shear velocity structure of the upper mantle globally and beneath North America. Journal of Geophysical Research 113, B02303 http://dx.doi.org/10.1029/2006JB004819.
Paige, C.C., Saunders, M.A., 1982. LSQR — an algorithm for sparse linear-equations and sparse least-squares. ACM Transactions on Mathematical Software 8 (1), 43–71.
Priestley, K., Debayle, E., McKenzie, D., Pilidou, S., 2006. Upper mantle structure of eastern Asia from multimode surface waveform tomography. Journal of Geophysical Research 111, B10304 http://dx.doi.org/10.1029/2005JB004082.
Qi, C., Zhao, D.P., Chen, Y., Chen, Q.F., Wang, B.S., 2006. 3-D P and S wave velocity structures and their relationship to strong earthquakes in the Chinese capital region. Chinese Journal of Geophysics-Chinese Edition 49 (3), 805–815.
Rudnick, R., Liu, J., Walker, R., Gao, S., Wu, F., Xu, W., 2011. Insights into craton formation and destruction from Re–Os isotopes and highly siderophile elements in peridotite xenoliths from the North China Craton. Abstract of the International Conference on Craton Formation and Destruction: Beijing, p. 3.
Santosh, M., 2010. Assembling North China Craton within the Columbia supercontinent: the role of double-sided subduction. Precambrian Research 178 (1–4), 149–167.
Santosh, M., Zhao, D.P., Kusky, T., 2010. Mantle dynamics of the Paleoproterozoic North China Craton: a perspective based on seismic tomography. Journal of Geodynamics 49 (1), 39–53.
Savage, M.K., 1999. Seismic anisotropy and mantle deformation: what have we learned from shear wave splitting? Reviews of Geophysics 37 (1), 65–106.
Silver, P.G., 1996. Seismic anisotropy beneath the continents: probing the depths of geology. Annual Review of Earth and Planetary Sciences 24, 385–432.
Smith, G.P., Ekstrom, G., 1999. A global study of P-n anisotropy beneath continents. Journal of Geophysical Research 104 (B1), 963–980.
Thurber, C., Ritsema, J., 2007. 1.10 — theory and observations — seismic tomography and inverse methods. In: Gerald, S. (Ed.), Treatise on Geophysics. Elsevier, Amsterdam, pp. 323–360.
Tian, Y., Zhao, D., 2011. Destruction mechanism of the North China Craton: insight from P and S wave mantle tomography. Journal of Asian Earth Sciences 42, 1132–1145.
Tian, Y., Zhao, D.P., Sun, R.M., Teng, J.W., 2009. Seismic imaging of the crust and upper mantle beneath the North China Craton. Physics of the Earth and Planetary Interiors 172 (3–4), 169–182.
Tsunogae, T., Liu, S.J., Santosh, M., Shimizu, H., Li, J.H., 2011. Ultrahigh-temperature metamorphism in Daqingshan, Inner Mongolia Suture Zone, North China Craton. Gondwana Research 20 (1), 36–47.
Wang, J., Zhao, D.P., 2008. P-wave anisotropic tomography beneath Northeast Japan. Physics of the Earth and Planetary Interiors 170 (1–2), 115–133.
Wang, J., Zhao, D.P., 2010. Mapping P-wave anisotropy of the Honshu arc from Japan Trench to the back-arc. Journal of Asian Earth Sciences 39 (5), 396–407.

Wang, J., Zhao, D.P., 2012. P wave anisotropic tomography of the Nankai subduction zone in Southwest Japan. Geochemistry, Geophysics, Geosystems 13, Q05017 http://dx.doi.org/10.1029/2012gc004081.
Wessel, P., Smith, W., 1998. New improved version of the Generic Mapping Tools released. EOS, Transactions of the American Geophysical Union 79, 579.
Wu, F.Y., Lin, J.Q., Wilde, S.A., Zhang, X.O., Yang, J.H., 2005. Nature and significance of the Early Cretaceous giant igneous event in eastern China. Earth and Planetary Science Letters 233 (1–2), 103–119.
Wu, F.Y., Walker, R.J., Yang, Y.H., Yuan, H.L., Yang, J.H., 2006. The chemical-temporal evolution of lithospheric mantle underlying the North China Craton. Geochimica et Cosmochimica Acta 70 (19), 5013–5034.
Wu, F.Y., Xu, Y.G., Gao, S., Zheng, J.P., 2008. Lithospheric thinning and destruction of the North China Craton. Acta Petrologica Sinica 24 (6), 1145–1174.
Xu, P.F., Zhao, D.P., 2009. Upper-mantle velocity structure beneath the North China Craton: implications for lithospheric thinning. Geophysical Journal International 177 (3), 1279–1283.
Xu, Y., Liu, F.T., Liu, J.H., Sun, R.M., 2001. Seismic tomography beneath the orogenic belts and adjacent basins of northwestern China. Science in China Series D: Earth Sciences 44 (5), 468–480.
Xu, Y.G., Chung, S.L., Ma, J.L., Shi, L.B., 2004. Contrasting Cenozoic lithospheric evolution and architecture in the western and eastern Sino–Korean craton: constraints from geochemistry of basalts and mantle xenoliths. Journal of Geology 112 (5), 593–605.
Yang, X.Z., Xia, Q.K., Deloule, E., Dallai, L., Fan, Q.C., Feng, M., 2008. Water in minerals of the continental lithospheric mantle and overlying lower crust: a comparative study of peridotite and granulite xenoliths from the North China Craton. Chemical Geology 256 (1–2), 33–45.
Yang, J.H., O'Reilly, S., Walker, R.J., Griffin, W., Wu, F.Y., Zhang, M., Pearson, N., 2010. Diachronous decratonization of the Sino–Korean craton: geochemistry Of mantle xenoliths from North Korea. Geology 38 (9), 799–802.
Zang, S., Yang, J., 1984. The depth distribution of North China intraplate earthquakes and their physical background. Seismology and Geology-Chinese Edition 6 (3), 67–75.
Zhai, M.G., Liu, W.J., 2003. Palaeoproterozoic tectonic history of the North China craton: a review. Precambrian Research 122 (1–4), 183–199.
Zhang, M., Zhou, X., Zhang, J., 1998. Nature of the lithospheric mantle beneath NE China: evidence from potassic volcanic rocks and mantle xenoliths. In: Flower, M., Chung, S., Lo, C., Lee, T. (Eds.), Mantle Dynamics and Plate Interactions in East Asia. Geodynamics Series. American Geophysical Union, pp. 197–220.
Zhang, H.F., Sun, M., Zhou, M.F., Fan, W.M., Zhou, X.H., Zhai, M.G., 2004. Highly heterogeneous Late Mesozoic lithospheric mantle beneath the North China Craton: evidence from Sr–Nd–Pb isotopic systematics of mafic igneous rocks. Geological Magazine 141 (1), 55–62.
Zhao, D.P., 2004. Global tomographic images of mantle plumes and subducting slabs: insight into deep Earth dynamics. Physics of the Earth and Planetary Interiors 146 (1–2), 3–34.
Zhao, L., Xue, M., 2010. Mantle flow pattern and geodynamic cause of the North China Craton reactivation: evidence from seismic anisotropy. Geochemistry, Geophysics, Geosystems 11, Q07010 http://dx.doi.org/10.1029/2010GC003068.
Zhao, D.P., Hasegawa, A., Horiuchi, S., 1992. Tomographic imaging of P and S wave velocity structure beneath Northeastern Japan. Journal of Geophysical Research 97 (B13), 19909–19928.
Zhao, D.P., Kanamori, H., Negishi, H., Wiens, D., 1996. Tomography of the source area of the 1995 Kobe earthquake: evidence for fluids at the hypocenter? Science 274, 1891–1894.
Zhao, G.C., Wilde, S.A., Cawood, P.A., Sun, M., 2001. Archean blocks and their boundaries in the North China Craton: lithological, geochemical, structural and P–T path constraints and tectonic evolution. Precambrian Research 107 (1–2), 45–73.
Zhao, D.P., Lei, J.S., Tang, R.Y., 2004. Origin of the Changbai intraplate volcanism in Northeast China: evidence from seismic tomography. Chinese Science Bulletin 49 (13), 1401–1408.
Zhao, G.C., Sun, M., Wilde, S.A., Li, S.Z., 2005. Late Archean to Paleoproterozoic evolution of the North China Craton: key issues revisited. Precambrian Research 136 (2), 177–202.
Zhao, D.P., Maruyama, S., Omori, S., 2007. Mantle dynamics of Western Pacific and East Asia: insight from seismic tomography and mineral physics. Gondwana Research 11 (1–2), 120–131.
Zhao, D.P., Tian, Y., Lei, J.S., Liu, L., Zheng, S.H., 2009. Seismic image and origin of the Changbai intraplate volcano in East Asia: role of big mantle wedge above the stagnant Pacific slab. Physics of the Earth and Planetary Interiors 173 (3–4), 197–206.
Zhao, G.C., He, Y.H., Sun, M., 2009. The Xiong'er volcanic belt at the southern margin of the North China Craton: petrographic and geochemical evidence for its outboard position in the Paleo-Mesoproterozoic Columbia Supercontinent. Gondwana Research 16 (2), 170–181.
Zhao, L., Allen, R.M., Zheng, T.Y., Hung, S.H., 2009. Reactivation of an Archean craton: constraints from P- and S-wave tomography in North China. Geophysical Research Letters 36, L17306 http://dx.doi.org/10.1029/2009GL039781.
Zhao, D.P., Santosh, M., Yamada, A., 2010. Dissecting large earthquakes in Japan: role of arc magma and fluids. Island Arc 19, 4–16.
Zheng, J.P., O'Reilly, S.Y., Griffin, W.L., Lu, F.X., Zhang, M., 1998. Nature and evolution of Cenozoic lithospheric mantle beneath Shandong peninsula, Sino–Korean craton, eastern China. International Geology Review 40 (6), 471–499.
Zheng, J.P., Griffin, W.L., O'Reilly, S.Y., Yu, C.M., Zhang, H.F., Pearson, N., Zhang, M., 2007. Mechanism and timing of lithospheric modification and replacement beneath the eastern North China Craton: peridotitic xenoliths from the 100 Ma Fuxin basalts and a regional synthesis. Geochimica et Cosmochimica Acta 71 (21), 5203–5225.
Zheng, T.Y., Zhao, L., Zhu, R.X., 2009. New evidence from seismic imaging for subduction during assembly of the North China craton. Geology 37 (5), 395–398.
Zhu, R.X., Zheng, T.Y., 2009. Destruction geodynamics of the North China craton and its Paleoproterozoic plate tectonics. Chinese Science Bulletin 54 (19), 3354–3366.